SIMULATION OF AUTONOMOUS LANDING NEAR A PLUME SOURCE IN A TIGER STRIPE CANYON ON THE SOUTH POLE OF ENCELADUS

Konstantinos Konstantinidis, Julian Adler, Robert Jacob, Paul Dykta, Manuel Thies, Martin Rudolph, Roger Förstner

Institute for Space Technology and Space Applications (ISTA), Bundeswehr University Munich, Germany

ABSTRACT

The Institute for Space Technology and Space Applications (ISTA) of Bundeswehr University Munich is investigating mission concepts for the in-situ astrobiological exploration of the icy moons of the outer solar system. A concept studied in the context of the DLR funded Enceladus Explorer project (EnEx) aimed to place a lander near one of the plume sources on the bottom of a "tiger stripe" canyon on the south pole of Saturn's moon Enceladus. Once there, the lander would deploy a melting probe to sample relatively shallow liquid water in the ice under the plume source. The lander would have to achieve a landing accuracy of 50 m and manage to land safely on an extremely challenging terrain interspersed with landing hazards like ice blocks, but also uncertain terrain like soft and unconsolidated snow or hard ice. To achieve this, a landing Guidance, Navigation, and Control (GN&C) system would be necessary to allow for autonomous landing operations. To achieve the required accuracy, terrain relative navigation can use sensors such as optical and thermal cameras, LIDAR, etc. to navigate relative to detected terrain features. To ensure a safe landing the system must be able to assess if the originally planned landing site is safe and if not, to then autonomously command a retargeting to another, safer spot. The guidance and control function must then calculate a viable trajectory and thrust arc to the newly chosen landing site. To validate that the landing satisfies the accuracy and reliability requirements we are developing a tool in Matlab/Simulink to simulate the operation of the autonomous landing GN&C system. In this paper we present a first version of this tool, used to simulate the final phase of landing operations as described above. It comprises the following parts:

Terrain simulation block: Generates a simple terrain model based on a given Digital Elevation Model (DEM) file. The topology can be modified using fractal algorithms and arbitrary simple shapes can be added to represent hazards. Terrain texture is also simulated.

SLAM block: Simulates Terrain Relative Navigation (TRN)/feature matching, whereby features are extracted from the simulated terrain and a Simultaneous Localization and Mapping (SLAM) approach is followed for accurate navigation.

Hazard Detection and Avoidance (HDA) block: Creates fused hazard maps from the output of camera and LIDAR sensors based on the simulated interaction of these sensors with the terrain. A fuzzy logic approach is used to evaluate landing safety and command a retargeting if necessary.

Guidance and control block: Implements E-guidance and D'Souza guidance algorithms to generate a thrust arc and trajectory to a new landing spot if commanded by HDA.

Using this tool we will attempt to show the feasibility of an adequately accurate and safe landing near a plume source on the bottom of a tiger stripe canyon on the south pole of Enceladus.

Index Terms **-** Autonomous landing, GN&C simulation, Enceladus, Icy moons, Astrobiology

1. ENCELADUS

Enceladus is currently seen as one of the prime candidates for hosting microbial life in the Solar system in the present day.

Enceladus is a small icy moon orbiting Saturn at a radius of 4 Saturn radii. Having a diameter of ≈ 500km, it was once believed too small to be active, but it has been found to be one of the most geologically dynamic objects in the Solar System [1]. It is characterized by a wide range of terrains, including old and young surfaces. It's most interesting area is at its south pole, where a geologically active province was identified by Cassini [2]. The most prominent feature at the South pole are four linear depressions, dubbed "tiger stripes" because of their appearance in the infrared. Multiple flybys of Cassini at Enceladus have shown that plumes of H_2O, including simple organic compounds [3], emanate via

cryovolcanism from those "warm" fractures at the tiger stripes. Analysis of the plume material strongly implies that it originates from a global ocean below its icy crust [4], and its unique chemistry has fueled speculation that Enceladus may harbor life [5].

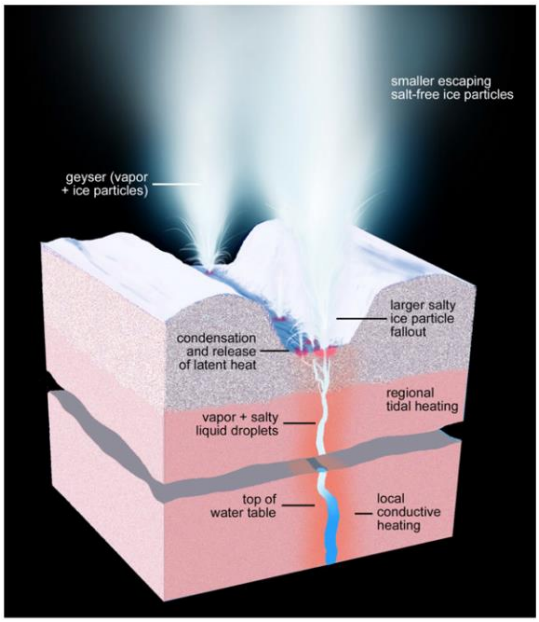

Figure 1: Schematic illustrating current knowledge of the small-scale physical and thermal structure and processes relevant to Enceladus' geysering activity [6]

1.1. TOPOGRAPHY AND ENVIRONMENT OF THE SOUTH POLAR TERRAIN (SPT)

The South-Polar Terrain is host to the plume sources. The most prominent features characterizing the interior of the SPT as mentioned above are the "Tiger Stripe" valleys, which include 101 identified distinct vapor and ice jets which form the plumes towering above Enceladus (Figure 1) [6]. The term "Tiger Stripe" describes a "V" shaped valley enclosed by two, nearly parallel ridges. These ridges are about 100–150 m high, while the valley is about 200–250 m deep. The total width of the formation is about 2–5 km. The South-Polar Terrain features 4 valleys (Damascus, Baghdad, Cairo and Alexandria Sulcus) separated from each other by 35 km wide plains. As one moves closer to a Tiger Stripe valley, the terrain rises with a relatively gentle gradient to the summits of the ridges. The terrain texture also changes from highly fractured to a more undulating one, covered with numerous icy blocks. Once over the lateral ridges, the slope is initially steeper but changes to a more moderate gradient the deeper one descends, with unconsolidated material sliding from steeper down to flatter sections, where material tends to accumulate. The valley floor is expected to be very narrow, in the order of 50–100 m [7], and interspersed with obstacles, such as narrow ridges and elongated domes. An indicative picture of the South-Polar Terrain at Enceladus can be seen in Figure 2. An elevation model of a characteristic canyon area on the SPT is shown in Figure 3.

The spatial density of ice-block features in the SPT was estimated for blocks larger than 10 m in [8]. Block density was found to be up to 1500 ± 450 blocks per square km. No distinct block distribution pattern was found with respect to the tiger-stripe flanks or jet sources.

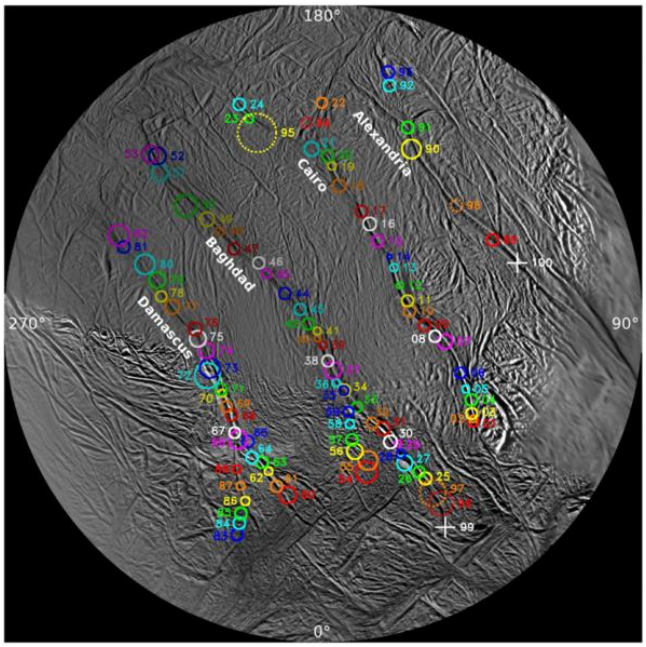

Figure 2: Polar stereographic map of Enceladus' South-Polar Terrain (SPT) showing the location of 100 plume sources. The circles are the 2σ uncertainties [6]

An important aspect is the texture of the surface material in the South-Polar Terrain. It is mainly the fallout from the plumes that modifies the texture: ice particles tend to accumulate more near the plumes and less further away. Studies have shown that nearer the plumes, particle deposition rates can reach up to 1 mm/year or more in the large scale and possibly more in smaller scales, indicating a deposit layer thickness of tens of meters if we assume that the plumes have been active in the past million years [9]. Still, exposed icy crust can also be encountered, especially on slopes on which less consolidated material has slid downward.

The mechanical behavior of the fallout is also crucial to the understanding of the surface texture. In a first approach the fallout can be approximately treated as super-fine snow,

comprising grains of about 7.5 µm outside the SPT, 40 µm in the vicinity of the Tiger Stripes and 100 µm or larger inside the valleys, where larger particles tend to fall nearer to the plumes [9]. Grains are expected to have lost their crystalline shape due to collisions with the vent walls, and have a roughly round shape. These microscopic properties are translated to macroscopic properties of the surface material, namely: increased force transmission capacity due to the fine grain size, non-consolidated layers of material and increased compressibility due to the low gravity.

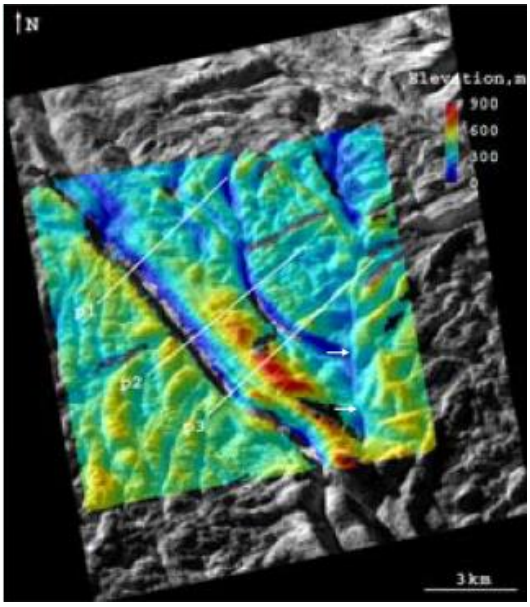

Figure 3: Stereo-derived elevation model of characteristic canyon area on the SPT, on Baghdad Sulcus (76°S / 323°E) [7]

The density of H_2O molecules in the vicinity of the plumes has been modelled in [10]. At the very mouth of the plume source the water vapor density is estimated in the order of 10^{22} molecules/m^3, dropping by 3 orders of magnitude within a distance of 100 m. To put these numbers into perspective it's instructive to compare them to the Earth's atmospheric density at sea level, $\rho_{Earth} = 10^{25}$ molecules/m^3, or to that of Mars, $\rho_{Mars} = 10^{23}$ molecules/m^3. The fresh, clean ice that dominates the surface of Enceladus gives it the most reflective surface of any body in the Solar System (albedo of 0.99).

2. THE ENCELADUS EXPLORER (ENEX) PROJECT AND THE ENCELADUS LANDER (EL) MISSION CONCEPT

Between 2012 and 2015 the joint research collaboration "Enceladus Explorer" (EnEx) funded by the German Space Administration (DLR), investigated the necessary technologies for a future exploration of the Saturnian moon Enceladus. The goal was the development of a terrestrial navigation system for a subglacial research probe. The EnEx consortium was led by FH Aachen University of Applied Sciences and consisted of eight German Universities.

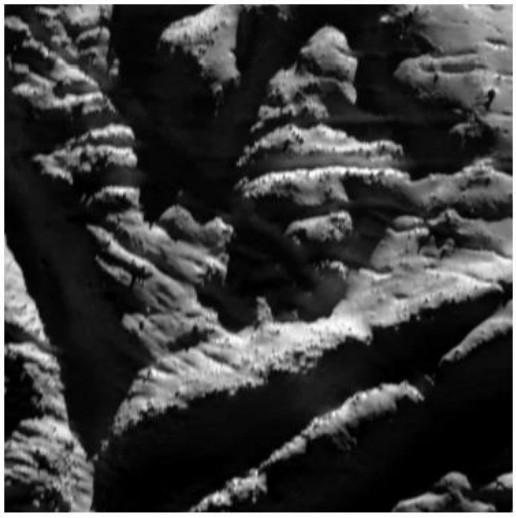

Figure 4: Rough terrain at Enceladus' south pole with boulders resting along the tops of high frozen ridges. Image credits: NASA/JPL/Space Science Institute, Universe Today

The developed navigation solution was integrated into a research melting probe of the IceMole type, a melting probe concept which has been developed at FH Aachen University of Applied Sciences since 2008. The IceMole probe was validated and tested during field tests conducted as part of an ongoing collaboration between EnEx and MIDGE, a NSF funded Antarctic exploration initiative [11].

In the context of the EnEx project, the Institute of Space Technology & Space Applications (ISTA) of the Bundeswehr University Munich was responsible for the overall mission and system concept for a mission to land near a plume at Enceladus and deploy the IceMole there. The mission scenario for the extraterrestrial application of such a probe was studied, in order to determine the conditions for the complete design and extraterrestrial operation of the navigation system in detail. The detailed Enceladus Lander (EL) mission concept created during the project is given in [12].

The EL mission concept has the aim to deploy a future version of the IceMole melting probe near one of the plumes of Enceladus. The EL mission comprises of three elements: an Orbiter, a Lander, and the IceMole. This Combined Spacecraft will transfer to Enceladus and communicate with

Earth, with the Orbiter serving as the propulsion module. For the transfer to Enceladus, a nuclear reactor on the Lander provides power to the electric propulsion system. After orbital capture around Enceladus, the Orbiter will perform remote sensing of potential landing sites during the landing site reconnaissance phase. Once landing site reconnaissance is completed by the Orbiter, the Lander will separate and land precisely and safely near one of the plume sources on the bottom of a tiger stripe canyon. After Lander separation, the main function of the Orbiter will be to relay data between lander and Earth. Once landed, the IceMole will be deployed. The thermal melting head of the IceMole will be powered by the nuclear reactor. Once the IceMole reaches a depth of 100 m or more close to the wall of water-filled fracture, it will sample liquid water within the fracture for biosignatures.

An illustration of the Lander is shown in Figure *5*.

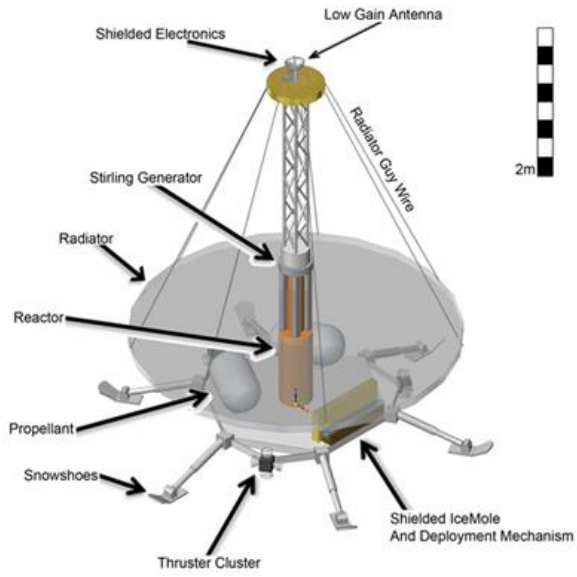

Figure 5: Design of the EL Lander

3. LANDING NEAR A PLUME SOURCE

The drivers for landing accuracy are the width of the canyon floor, at around 100 m, and the desire to minimize the length of the tether connecting the IceMole to the Lander for power and communications purposes. Landing too close to the plume source should also be avoided to minimize planetary protection related concerns (see [13]). Taking these considerations into account, the target landing area shall be circle with a radius smaller than 50 m. Such a landing accuracy is categorized as pinpoint landing (see e.g. [14]).

As seen in Sec. 1.1, the landing area is also expected to be strewn with hazards such as ice blocks, cracks, domes, unconsolidated materials, etc. that are too small to be identified from orbit. Due to the uncertainty of the terrain, real-time hazard detection is necessary, as well as logic for the avoidance of landing hazards.

To give context to the following, the GN&C system used during descent and landing operations will be briefly described here.

Figure 6 gives the top-level architecture of the GN&C system for landing. Terrain relative navigation instruments in conjunction with conventional navigation instruments help accurately navigate the lander during landing. During the final landing phases, data from terrain relative instruments is also used to detect and avoid landing hazards. Control of the calculated trajectory and attitude is then performed using the Lander's propulsion system.

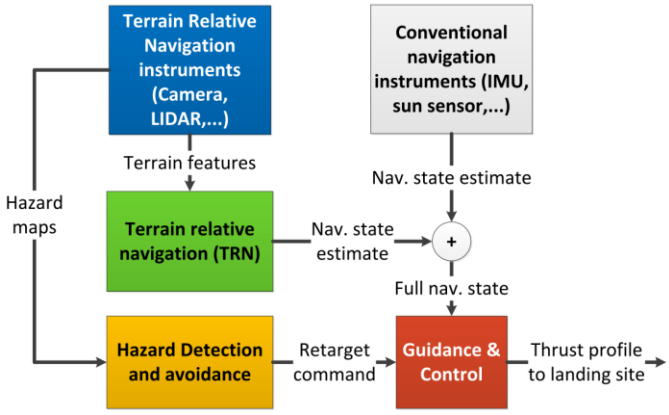

Figure 6: Illustration of a top-level GN&C system architecture

Figure 7 illustrates the Descent and Landing sequence. The landing operational sequence was based on that of the ESA Lunar Lander mission [15][16][17]. The landing sequences of other icy moon landing missions with similar accuracy requirements were taken into account [18] [14].

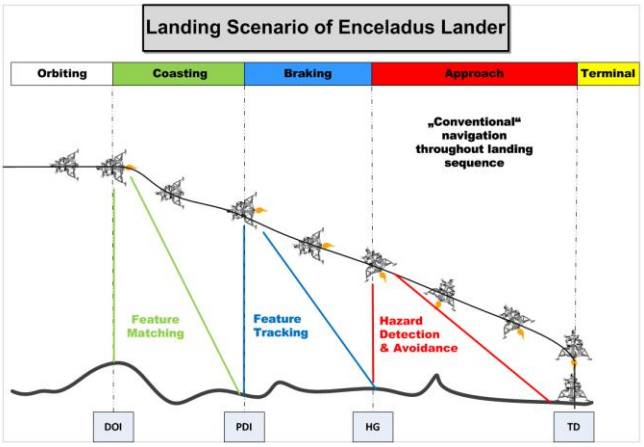

Figure 7: Operations concept for landing phase

The reference landing scenario is divided into separate phases:

Lander separation: The reference scenario starts in the 200 km Enceladus Reconnaissance orbit, after separation between the Lander and the Orbiter has been successfully performed.

Coasting phase: The Descent Orbit Insertion (DOI) marks the start of the descent phase. This is short burn by the main engines of the lander to go on a Hohmann transfer orbit and periapsis of 5 km. During the coasting phase up to periapsis, feature matching TRN is performed to increase precision of state estimation.

Braking phase: At periapsis the Powered Descent Initiation (PDI) meaning that the main engine is turned on for the main braking phase most of the orbital velocity is eliminated, from orbital speeds to about 100 m/s. During or shortly after the main braking, the landing site will come into the field of view of the camera. This marks High Gate (HG).

Approach phase: Once the Lander has achieved a sufficiently reduced velocity the engines begin to throttle down and the approach phase begins, starting targeted descent towards the selected landing spot. During this phase the Hazard Detection and Avoidance (HDA) function is active. If the designated landing spot proves unsuitable, retargeting can take place and a new landing spot within the Lander's reach selected. The spacecraft will perform feature tracking TRN, complemented with IMU measurements during this phase.

Touch down: Once the Lander is above the landing site with no horizontal velocity and a vertical attitude at an altitude of 10-20 m (Terminal Gate, TG), it shuts it engines and slowly free-falls to a soft Touchdown (TD) on the surface.

In this work, we have identified the approach phase as the most critical, since it is the phase where critical hazard detection and avoidance takes place. Therefore, in the following we will focus only on this phase.

4. LANDING SIMULATION

To confirm the feasibility of landing on Enceladus with the set requirements, we are developing a tool in Matlab/Simulink to simulate the operation of the autonomous landing GN&C system. The landing simulation tool and its constituent parts are illustrated in Figure 11 and will be described in the following. As mentioned above, the tool focuses on the approach phase, as the most critical.

4.1. TERRAIN SIMULATION BLOCK

The target area for the EL lander is one of the plume sources on the bottom of a tiger stripe canyon on the south pole of Enceladus. As described in sec. 1.1, this is a very challenging terrain to land on.

The purpose of this tool block is to generate adequately realistic simulated terrains that can be used for the purpose of simulating the TRN and HDA functions. To achieve that, the block performs a number of steps. First an area on Earth is chosen that a) resembles the canyon terrain on the SPT as described in sec. 1.1, and b) has high-resolution elevation data available for download. The Digital Elevation Model (DEM) for this area is then downloaded and plotted using Matlab's Mapping Toolbox. The surface of Enceladus and particularly the SPT is dominated by water ice and is characterized by an albedo of almost 1. The DEM is thus simply given a white color. To simulate terrain illumination and shading, we use the Shadem Matlab function [19], that shades a given terrain model based on the input Sun azimuth and elevation.

DEMs for Earth usually come at a resolution of 1m per pixel. In case greater resolution is needed for the landing simulation the block must be able to increase the DEM resolution by adding extrapolated elevation data points between the ones given in the DEM. To achieve this a diamond-square algorithm is used [20], as applied in Matlab [21].

Another important aspect of the terrain is the landing hazards: ice blocks of varying sizes, and hazardous surface texture like soft snow and rugged ice. The first type of hazards is to be simulated by generating randomly shaped objects and distributing them around the terrain according to the proper and size spatial distributions as discussed in sec. 1.1. The second type is going to be simulated by flagging certain areas on the surface as hazardous.

4.2. TERRAIN RELATIVE NAVIGATION (TRN) BLOCK

In order for the lander to achieve its demanding accuracy requirements it will need a terrain relative navigation function. In this tool we will use a Simultaneous Localization And Mapping (SLAM) approach for TRN.

SLAM is a method by which a robot constructs a map of landmarks of its surrounding world, which it uses at the same time to localize itself in it.

SLAM consists of mainly two parts that take place during each iteration step: feature extraction and matching, and lander state estimation and update, and feature update. The two functions and the methods we are considering to implement them are described in the following.

4.2.1. Feature detection and matching

In order to allow for distinctive feature detection and matching on a planetary surface, we have implemented an improved modification of the Scale Invariant Feature Transform (SIFT). The basic principle of the method is Gaussian filtering of camera images in multiple scales.

Hereafter, neighboring images in the scale space are subtracted to create the Difference-of-Gaussian Scale Space (DOG).

From this point, pixels are compared with their neighboring pixels, including the adjacent scale images. If a pixel turns out to be a minimum or maximum by its value, it is initially detected as a distinctive feature. A Taylor expansion of the DOG Scale Space up to quadratic terms may be used to locate the features with sub-pixel accuracy.

Based on local DOG Scale Space gradient evaluation, weak keypoints are removed by a predetermined threshold and descriptor arrays are assigned to those keypoints which remain in the keypoint selection. The descriptor is determined by the main gradient direction and magnitude around the keypoint. This is used as a reference in comparison with other keypoints and enables the method to be invariant to image rotation. Hereafter, the local image gradients in a certain region around the keypoint are added to a descriptor array for each feature. A nearest neighbour search in the descriptor space finally allows for matching of the keypoints [22–24].

4.2.2. Extended Kalman Filter (EKF) SLAM

As soon as the landmark extraction and the feature detection and matching is in place, the SLAM process can be summarized in the following steps, as shown in Figure 9:

1. perception of new landmarks and their initialization in the map,
2. prediction of robot motion with associated increase of its position uncertainty,
3. observation of already mapped landmarks from an uncertain robot position, and
4. correction of landmark positions and robot localization, with associated decrease of both robot, and map uncertainties.

The process is described in more detail in [25].

For our tool, we adapted the open source SLAM-Toolbox developed by Joan Solá written in Matlab [26]. The toolbox is described in [25].

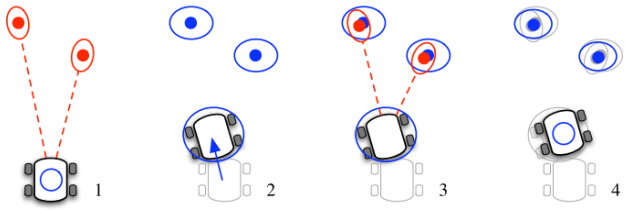

Figure 9: Typical SLAM operations during a complete filter loop. For explanation see text. Ellipses represent the uncertainty boundaries [25].

4.3. HAZARD DETECTION AND AVOIDANCE (HDA) BLOCK

In order to achieve landing with an adequate reliability on the challenging terrain near the bottom of a tiger stripe canyon, a capable HDA function must be implemented. HDA can be broken down to two sub-functions [27]:

- **Hazard mapping**, referring to the process of analyzing terrain topography and detecting hazards through image processing algorithms applied to navigation sensor input, and
- **Piloting**, referring to the concepts of data fusing, planning and decision-making used for the selection of a safe landing site.

In this work, we have adapted the Fuzzy rule based HDA method described in [28–30]. Here, we will discuss the

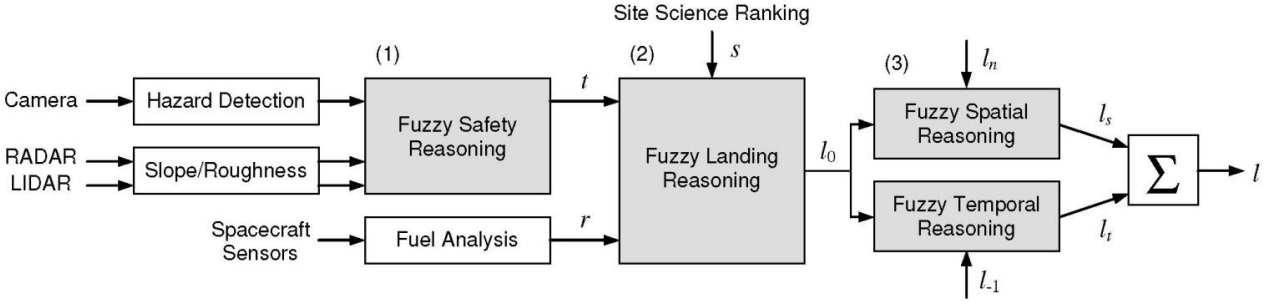

Figure 8: Block diagram of the selected Piloting approach. The three phases of reasoning are shown in gray [28]

methods we used to implement these functions in our tool.

4.3.1.Hazard mapping

For hazard mapping, on-board sensors sense the terrain to detect hazards. Multiple sensors are used (LIDAR, optical camera) for robustness. A combination of terrain features derived directly from the sensor measurements (e.g. slope, roughness) are used together with terrain features obtained by landmark detection algorithms (e.g. ice blocks). A hazard map can thus be created from each instrument. Example hazard maps from each instrument are shown in Figure 10.

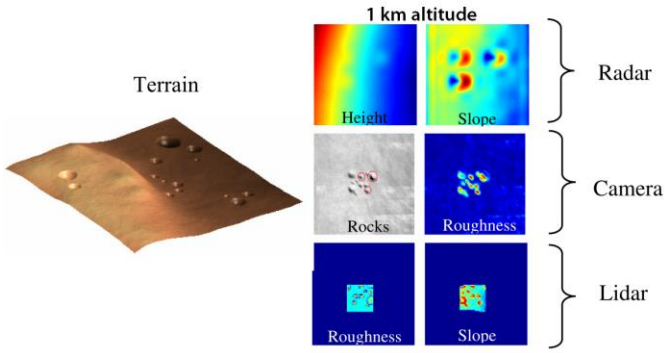

Figure 10: Example terrain (left) and extracted features at an altitude of 1km above the target landing site (right). Adapted from [29]

4.3.2.Piloting

Piloting will perform the decision process to assess whether retargeting is necessary.

Geological terrain characteristics identified from sensor data as discussed above must be combined to determine the risk associated with landing within the landing ellipse with the given terrain characteristics.

The selected Piloting approach is shown in Figure 8. It involves three stages of reasoning. At the first stage, the output of the hazard sensors is fused to a single hazard map. On the second stage, constraints such as the science value of landing sites and the reachability of each landing site candidate from the current lander state are included in the decision process, and a new map is generated incorporating this new information to the hazard map. The third stage investigates the spatial and temporal variability of the assigned landing site "goodness" values (a "good" landing site being safe, scientifically interesting, and easy to reach), that is, investigates whether a landing site remains good over many iterations, and whether the neighboring terrain is also considered good for landing. These two parameters confirm whether a landing site is indeed good.

The landing score incorporates the three key landing factors (terrain safety, fuel consumption, and scientific return), as well as spatial and temporal information that mitigates spurious sensor measurements. Site selection merely involves finding the point on the terrain with the highest score. A landing site which has the maximum landing score can be used to retarget the spacecraft and ensure a successful landing.

For the planetary landing Piloting problem, three different methods that can be used in each reasoning stage have been considered in the literature: fuzzy reasoning, probabilistic reasoning, and evidential reasoning [29]. For this problem, the design drivers are the short reaction times necessary, and the low computational power of on-board computers. Thus, to enable the necessary real-time implementation, fuzzy reasoning is chosen for all three stages. Fuzzy logic is a form of reasoning that is approximate rather than fixed and exact. Compared to traditional binary sets (where variables may take on true or false values), fuzzy logic variables may have a truth value that ranges in degree between 0 and 1. When linguistic variables are used (e.g. very dangerous, dangerous, safe), these degrees may be managed by specific functions [31]. Fuzzy sets and conditional statements allow the system to manage rule-based knowledge, imprecise information from sensors, and the uncertainties in the knowledge about the environment. Also importantly, fuzzy rule statements model the human expert's domain knowledge and can thus intuitively understood. Fuzzy logic rule evaluation involves only simple arithmetic calculations and conditional statements that can be performed very rapidly. Therefore, the computational time required for the reasoning process is quite manageable for a real-time decision system, making it feasible for landing operations [29].

An alternative, more robust but also more computationally expensive approach is to use all three of the reasoning methods mentioned above for each of the three stages of reasoning. The results from each method can then be fused, using e.g. a weighted average of the values from each method, giving a more robust result. This process is called Decision Fusion and is currently not implemented in our tool.

4.3. GUIDANCE AND CONTROL (G&C) BLOCK

The G&C function determines a suitable trajectory and thrust arc for the lander to reach the chosen landing site. The general guidance problem can be formulated as a two point boundary value problem (TPBVP), starting at the initial lander state and ending at the final lander state over the chosen landing site, with a lander velocity of zero and a vertical attitude.

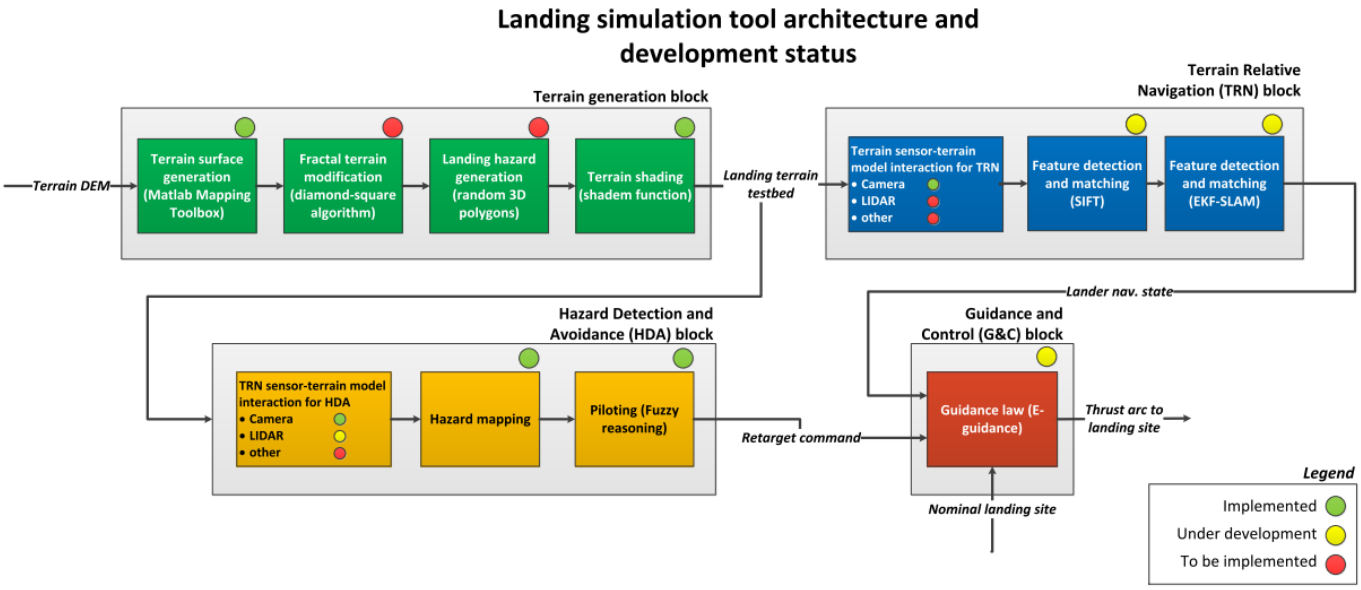

Figure 11: Landing simulation tool - architecture and development status

We compared several guidance algorithms and we selected to implement the Explicit or E-Guidance law, as given in [32]. This guidance law provides a universal solution of the two boundary-value planetary landing problem. It determines the required allocation of thrust along the controlled coordinate axis. The algorithm can be extended to take the final attitude into account as a constraint. The derivation of the required thrust is based on an algebraic linear polynomial approach.

We implemented E-guidance in Matlab/Simulink.

5. TOOL DEVELOPMENT STATUS AND INITIAL SIMULATION RESULTS

The architecture of the landing simulation tool and its development status are shown in Figure 11. This diagram also shows which parts of the tool we have already implemented, which parts need more development, and which parts we plan to implement. Some initial results will be presented here.

An example simulated terrain is shown in Figure 12, side to side with a closely imaged SPT terrain. The tool appears to be capable of generating Terrains that emulate the SPT quite satisfactorily.

The TRN block functions were also tested. Figure 13 demonstrates feature extraction and matching on two images of the same area on the surface of Jupiter's satellite Europa using the SIFT method we adapted. Figure 14 shows the lander trajectory and TRN camera sensor view, as implemented in the SLAM toolbox. Figure 15 shows some indicative navigation state results from the SLAM-toolbox.

A fused hazard map of a random terrain is given as an example in Figure 16.

Figure 17 shows some indicative trajectories and thrust arcs as generated by the G&C block, as well as trajectories before and after a retargeting to a better landing site is commanded by the HDA function.

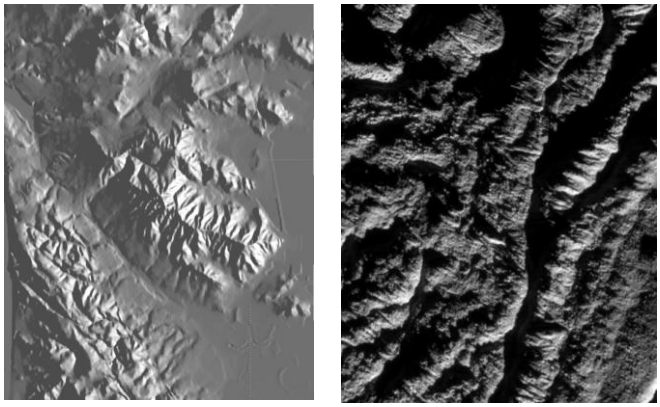

Figure 12: Left: Enceladus simulated terrain model as created using the Terrain Simulation Block. Right: SPT terrain as photographed by Cassini for comparison.

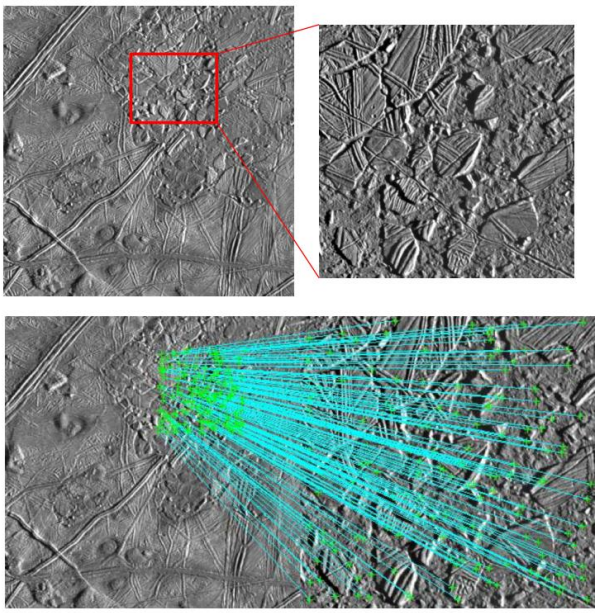

Figure 13: Application of the adapted SIFT feature extraction method on images showing the same area on Europa in different resolution

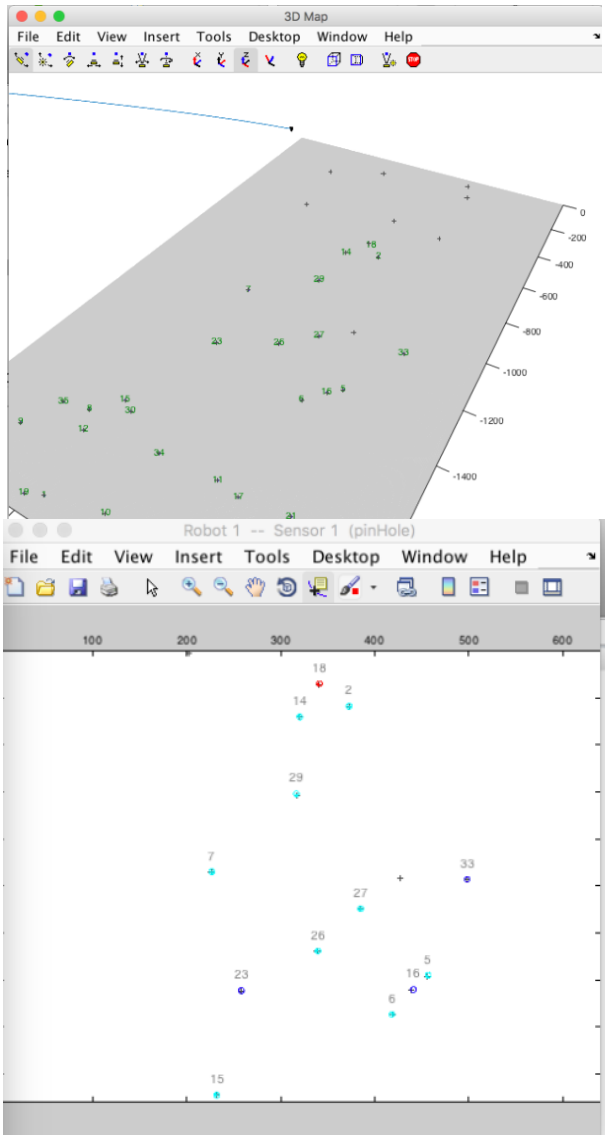

Figure 14: Top: Lander trajectory in SLAM-toolbox over arbitrary landmarks. Bottom: The view from the simulated camera sensor on the lander

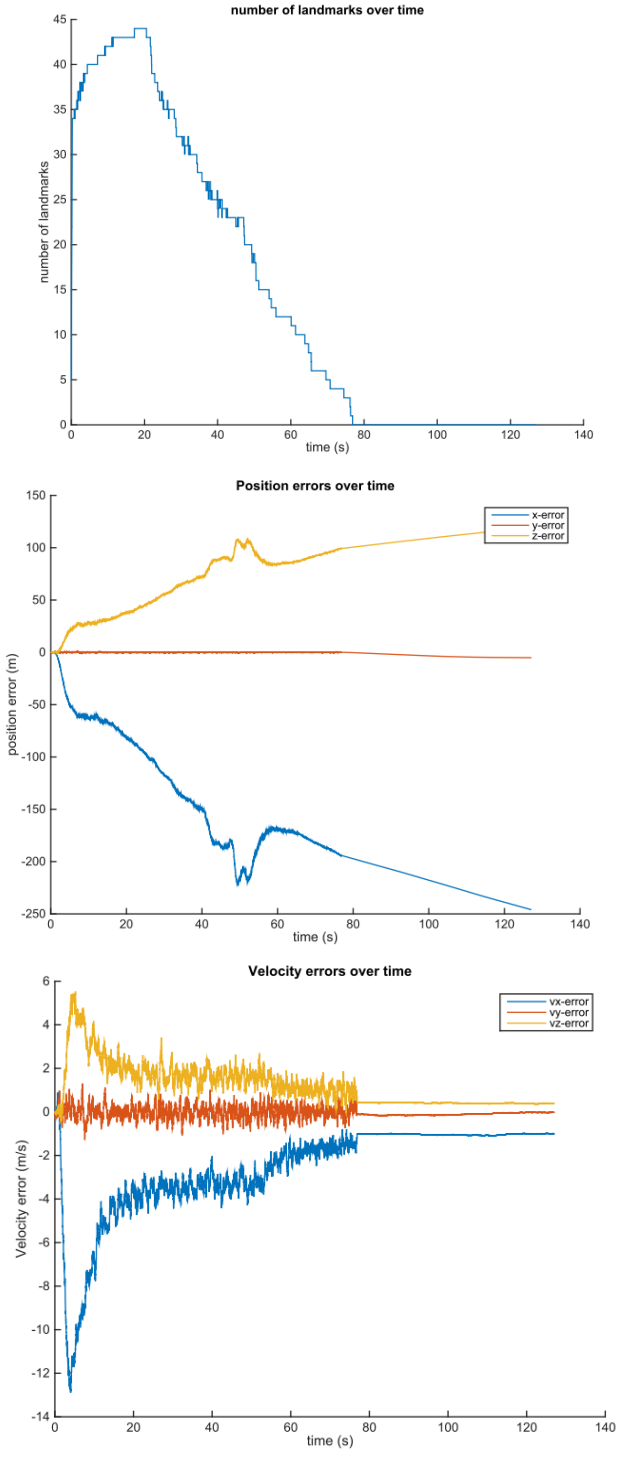

Figure 15: Indicative navigation state results using the SLAM toolbox. Top: number of landmarks used over time, Middle: position error over time, Bottom: velocity error over time

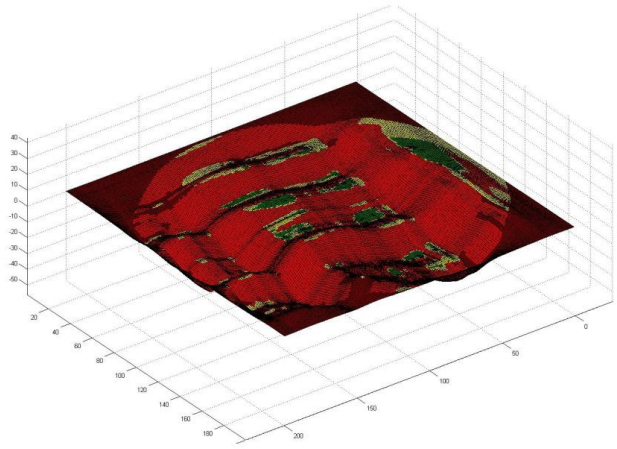

Figure 16: Fused hazard map for random simulated terrain shown in Figure 12

6. CONCLUSIONS AND FUTURE WORK

In this paper we present the work we have done so far towards creating a tool for simulating pinpoint safe landing on the bottom of a tiger stripe canyon on the SPT of Enceladus. We have made significant progress towards that goal, but several steps remain to be taken, as seen in Figure 11.

As two of the four main functions rely on the terrain model, it is very important to implement the remaining functionalities for the terrain generator. Thus we will be able to produce highly realistic terrain testbeds on which to simulate landing.

Work on the TRN and HDA blocks is to be continued, and their functionalities should be fully implemented. Simulations will show whether the accuracy and landing reliability requirements are satisfied. If that is not the case, additional sensors can be added, e.g. a thermal camera, to both help with navigating relative to the localized hotspots near the plumes, as well as contribute to the hazard map by detecting hazards due to their possible thermal inertia contrast against the surrounding environment. It should also be investigated what sensors are optimal for detecting surface texture hazards, e.g. soft, unconsolidated snow.

Using the tool we plan to also investigate whether the chosen guidance law and piloting method are indeed the optimal ones, and possibly implement and test novel solutions for either/both.

Finally we aim to eventually use the completed version of the tool to investigate ways to increase the robustness of the landing system, so that the lander can deal with the unprecedented accuracy and reliability requirements stemming from the target terrain's general roughness and

low illumination (polar region), as well as from its sensitivity as far as planetary requirements are concerned.

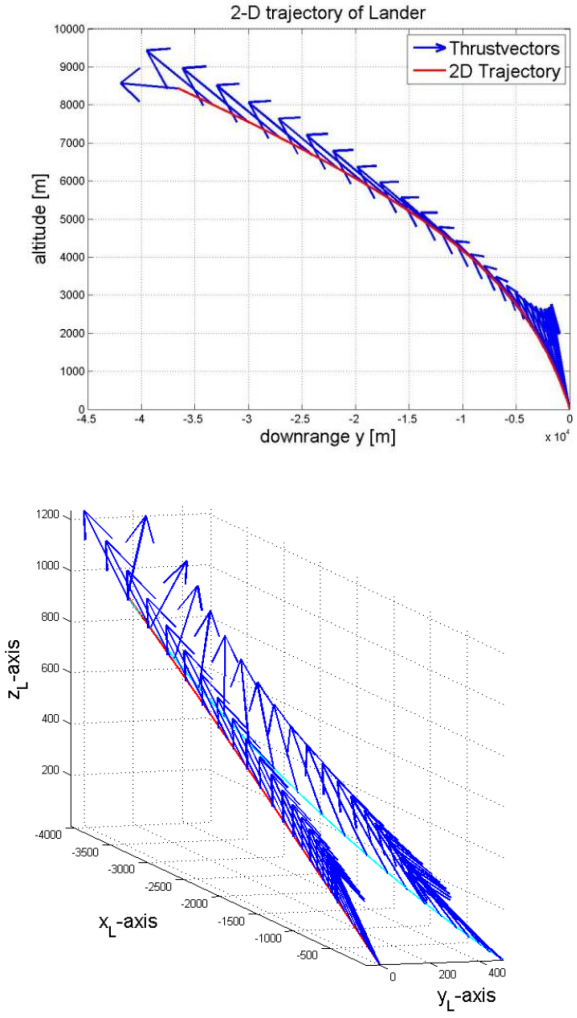

Figure 17: Top: Example trajectory and thrust arc as generated by the G&C block. Indicative trajectories and thrust arcs generated by the G&C block, before, and after a retarget maneuver as commanded by the HDA block

10. REFERENCES

[1] J.S. Kargel, Enceladus: cosmic gymnast, volatile miniworld., Science. 311 (2006) 1389–1391. doi:10.1126/science.1124495.

[2] C.C. Porco, P. Helfenstein, P.C. Thomas, A.P. Ingersoll, J. Wisdom, R. West, et al., Cassini observes the active south pole of Enceladus., Science. 311 (2006) 1393–1401. doi:10.1126/science.1123013.

[3] J.H. Waite Jr, W.S. Lewis, B. a. Magee, J.I. Lunine, W.B. McKinnon, C.R. Glein, et al., Liquid water on Enceladus from observations of ammonia and 40Ar in the plume, Nature. 460 (2009) 487–490. doi:10.1038/nature08153.

[4] D.A. Patthoff, S. a. Kattenhorn, A fracture history on Enceladus provides evidence for a global ocean, Geophys. Res. Lett. 38 (2011) n/a–n/a. doi:10.1029/2011GL048387.

[5] C.P. McKay, C.C. Porco, T. Altheide, W.L. Davis, T. a Kral, The possible origin and persistence of life on Enceladus and detection of biomarkers in the plume., Astrobiology. 8 (2008) 909–19. doi:10.1089/ast.2008.0265.

[6] C. Porco, D. DiNino, F. Nimmo, How the Geysers, Tidal Stresses, and Thermal Emission across the South Polar Terrain of Enceladus are Related, Astron. J. 148 (2014).

[7] B. Giese, P. Helfenstein, P.C. Thomas, A.P. Ingersoll, J. Perry, G. Neukum, et al., The morphology of an active zone near Enceladus ' south pole and implications, 12 (2010) 11085.

[8] H.R. Martens, A.P. Ingersoll, S.P. Ewald, P. Helfenstein, B. Giese, Spatial distribution of ice blocks on Enceladus and implications for their origin and emplacement, Icarus. 245 (2015) 162–176. doi:10.1016/j.icarus.2014.09.035.

[9] S. Kempf, U. Beckmann, J. Schmidt, How the Enceladus dust plume feeds Saturn's E ring, Icarus. 206 (2010) 446–457. doi:10.1016/j.icarus.2009.09.016.

[10] B. J. Hanna et al., Free Molecular and Collisional Studies of Enceladus' Water Vapor Plumes, 40th Lunar Planet. Sci. Conf. (2009).

[11] NSF Award Abstract Web-page: MIDGE: Minimally Invasive Direct Glacial Exploration of Biogeochemistry, Hydrology and Glaciology of Blood Falls, McMurdo Dry Valleys, (n.d.).

[12] K. Konstantinidis, C.L. Flores Martinez, B. Dachwald, A. Ohndorf, P. Dykta, P. Bowitz, et al., A lander mission to probe subglacial water on Saturn's moon Enceladus for life, Acta Astronaut. 106 (2015) 63–89. doi:10.1016/j.actaastro.2014.09.012.

[13] K. Konstantinidis, C. Hager, Enceladus Scenario and Operations – Operations Concept, 2014.

[14] Europa Study 2012 Report, Europa Lander Mission, NASA JPL, 2012.

[15] J. Delaune, D. De Rosa, S. Hobbs, Guidance and Control system design for Lunar Descent and

Landing, AIAA Guid. Navig. Control Conf. (2010) 1–10. doi:10.2514/6.2010-8028.
[16] E. Zaunick, D. Fischer, I. Ahrns, G. Orlando, B. Polle, E. Kervendal, Innovative Visual Navigation Solutions for ESA's Lunar Lander Mission, Presentation at the 9th International Planetary Probe Workshop, Toulouse June 21th, 2012.
[17] I. Gerth, E. Mooij, Guidance for Autonomous Precision Landing on Atmosphereless Bodies (under Review), AIAA J. (2014).
[18] A.I. Razzaghi, ed., Enceladus Flagship Mission Concept Study, NASA Goddard Space Flight Center, 2007.
[19] C. Greene, shadem Matlab function - Mathworks File Exchange, (2015).
[20] P. Martz, Generating Random Fractal Terrain - www.gameprogrammer.com/fractal.html, (1997).
[21] Fractal landscape generation with diamond-square algorithm - Mathworks File Exchange, (2013).
[22] R. Hartley, A. Zisserman, Multiple View Geometry in Computer Vision, Second Edi, Cambridge University Press, 2004.
[23] Lowe, Distinctive Image Features from Scale-Invariant Keypoints, (2004).
[24] Lowe, Object Recognition from Local Scale-Invariant Features, (1999).
[25] J. Solà-Ortega, Towards Visual Localization, Mapping and Moving Objects Tracking by a Mobile Robot: a Geometric and Probabilistic Approach - PhD Thesis, 2007.
[26] Joan Sola personal website: www.joansola.eu/, (n.d.).
[27] F. Câmara, P. Rogata, Hazard avoidance techniques for vision based landing, 6th Int. ESA …. 2005 (2005) 17–20.
[28] N. Serrano, H. Seraji, Landing Site Selection using Fuzzy Rule-Based Reasoning, (2007) 10–14.
[29] N. Serrano, M. Bajracharya, a. Howard, H. Seraji, A Novel Tiered Sensor Fusion Approach for Terrain Characterization and Safe Landing Assessment, 2006 IEEE Aerosp. Conf. (2006) 1–10. doi:10.1109/AERO.2006.1655795.
[30] a. Howard, H. Seraji, Multi-sensor terrain classification for safe spacecraft landing, IEEE Trans. Aerosp. Electron. Syst. 40 (2004) 1122–1131. doi:10.1109/TAES.2004.1386868.
[31] J. Novák, V., Perfilieva, I. and Močkoř, Mathematical principles of fuzzy logic, Dodrecht, 1999.
[32] G. CHERRY, A general, explicit, optimizing guidance law for rocket-propelled spaceflight, Astrodyn. Guid. Control Conf. Guid. Navig. Control Co-Located Conf. (n.d.).